V International Conference on Particle-based Methods – Fundamentals and Applications
PARTICLES 2017
P. Wriggers, M. Bischoff, E. Oñate, D.R.J. Owen, & T. Zohdi (Eds)

ENERGY BALANCE IN A PARTICLE SYSTEM

ARNO MAYRHOFER[1], ALICE HAGER[1] AND CHRISTOPH KLOSS[1]

[1]DCS Computing GmbH
Industriezeile 35, 4020 Linz
{arno.mayrhofer, alice.hager, christoph.kloss}@dcs-computing.com

Key words: DEM, Energy balance, Time integration.

Abstract. The energy distribution inside a particle system can be used to study the mechanical properties of such a system and its response to external perturbations. In the present article, the energy terms for typical discrete element models are derived. The derivation considers both Euler and Verlet integration schemes. Exemplary simulations are shown to demonstrate the validity of the derived formulation.

1 INTRODUCTION

The discrete element model (DEM) [1] is a widely used discrete model to simulate granular flows and has found its way from academia to industry. The DEM calculates the interaction of particles that are represented as volume elements (mostly spheres). To compute the interaction forces between two particles different variations of spring-damper systems are generally employed. As shown by [2] these models might cause artificial energy dissipation. However, [3] showed that explicit tracking of the dissipative energy is required and highlighted mistakes in earlier energy formulae, providing corrected formulations for Euler schemes. [4] also investigated energy in granular flows for comparably simple DEM models.

In the following the calculation of different energy terms in spring-damper systems is analysed using the standard Euler integration scheme. This is then followed by an extension to the velocity Verlet scheme, which is used in the LIGGGHTS® software. This will demonstrate the importance of the time integration scheme. Equipped with the general formulation several DEM models, from simple normal and lubrication models to a rather complicated bond model, will be reviewed.

The theoretical developments will be applied to four distinct test cases that show the validity of the present formulation and potential application areas. The first such area is model development and the second being the gaining of insight into the bulk. The latter can, for example, be used in engineering applications to determine energy usage of processes such as dredging.

2 DERIVATION

2.1 Euler scheme

Consider two particles that do not interact with each other at time t_0 and have no history of previous contacts. Then the total energy, assuming zero potential energy, of one particle is given by

$$\mathrm{E}_0 = \mathrm{E}_{\mathrm{kin},0} + \mathrm{E}_{\mathrm{pot},0} = \frac{\mathrm{m}\mathrm{v}_0^2}{2} \,. \tag{1}$$

The numeral subscripts denote the corresponding time step in the following and E_{kin} and E_{pot} are the kinetic and potential energy. v and m denote the velocity and mass of a particle, respectively. The Euler integration scheme reads

$$v_{i+1} = v_i + \frac{\Delta t}{m_i} F(x_i, v_i), \tag{2}$$

$$x_{i+1} = x_i + \Delta t \, v_i, \tag{3}$$

where x represents a particle position, Δt the time step size and $F(x_i, v_i)$ the forces computed based on the respective position and velocity.

Let the particles at time t_1 (with $\Delta t = t_1 - t_0$) interact with each other. The time integration of the velocity can also be written as

$$v_1 = v_0 + \frac{\Delta t\left(F_{e,0} + F_{d,0} + F_{ext,0}\right)}{m} \,, \tag{4}$$

where $F_{e,0}$, $F_{d,0}$ and $F_{ext,0}$ are the elastic, damping and external forces, respectively. The subscript 0 will be dropped for forces until the end of this section. The kinetic energy at t_1 can be written, using Eq. (4), as

$$E_{kin,1} = \frac{m v_1^2}{2} = \frac{m}{2}\left(v_0 + \frac{\Delta t}{m}\left(F_e + F_d + F_{ext}\right)\right)^2 . \tag{5}$$

Expansion of the right-hand side yields

$$E_{kin,1} = \frac{m}{2} v_0^2 + v_0 \Delta t F_e + v_0 \Delta t F_d + v_0 \Delta t F_{ext} + \frac{m}{2}\frac{\Delta t^2}{m^2} F_0^2 \,, \tag{6}$$

where F_0 is the sum of all forces acting on a particle. Shifting all terms from the left to the right, except for the kinetic energy one obtains

$$\frac{m}{2} v_1^2 - v_0 F_e \Delta t - v_0 F_d \Delta t - v_0 F_{ext} \Delta t - \frac{1}{2m} \Delta t^2 F_0^2 = \frac{m}{2} v_0^2 = E_{kin,0} = E_0. \tag{7}$$

Due to conservation of energy it is clear that the right-hand side is equal to E_1, i.e. the total energy of the system at time t_1. A DEM system is generally described using particles with a spring-damper interaction. Thus, the total energy can be split into four components:

$$E_1 = E_{kin,1} + E_{el,1} + E_{d,1} + \mathrm{E}_{\mathrm{pot},1}, \tag{8}$$

where $E_{el,1}$, $E_{d,1}$ and $E_{pot,1}$ are the elastic potential, dissipated and potential energy, respectively. The elastic potential energy E_{el} at time j is in general given by

$$E_{el,j} = -\sum_{i=0}^{j-1} v_{\alpha,i} F_{e,i} \Delta t \,, \tag{9}$$

where $v_{\alpha,i} = \alpha v_{\mathrm{i}+1} + (1-\alpha) v_{\mathrm{i}}$ and $\alpha \in [0,1]$. A similar argument holds for $E_{d,\mathrm{j}}$ and so

the energy budget can be written as

$$E_1 = \frac{m}{2} v_1^2 - v_\alpha F_{e,0} \Delta t - v_\beta F_{d,0} \Delta t - v_\gamma F_{ext} \Delta t. \tag{10}$$

Expanding the velocities yields

$$\begin{aligned} E_1 = \frac{m}{2} v_1^2 &- \alpha v_1 F_e \Delta t - (1-\alpha) v_0 F_e \Delta t \\ &- \beta v_1 F_d \Delta t - (1-\beta) v_0 F_d \Delta t \\ &- \gamma v_1 F_{ext} \Delta t - (1-\gamma) v_0 F_{ext} \Delta t \,, \end{aligned} \tag{11}$$

or

$$\begin{aligned} E_1 = \frac{m}{2} v_1^2 &- v_0 F_e \Delta t - v_0 F_d \Delta t - \mathrm{v}_0 F_{ext} \Delta t \\ &- \alpha (v_1 - v_0) F_e \Delta t - \beta (v_1 - v_0) F_d \Delta t - \gamma (v_1 - v_0) F_d \Delta t. \end{aligned} \tag{12}$$

The previously derived equation for $E_0 = E_1$ (Eq. (7)) can be recast slightly to read

$$\begin{aligned} E_1 = \frac{m}{2} v_1^2 &- v_0 F_e \Delta t - v_0 F_d \Delta t - v_0 F_{ext} \Delta t \\ &- \frac{1}{2m} \Delta t^2 \mathrm{F}_0 F_e - \frac{1}{2m} \Delta t^2 \mathrm{F}_0 F_\mathrm{d} - \frac{1}{2\mathrm{m}} \Delta \mathrm{t}^2 \mathrm{F}_0 \mathrm{F}_\mathrm{ext}. \end{aligned} \tag{13}$$

Equating these two expressions and removing the identical terms yields

$$\begin{aligned} -\frac{1}{2m} \Delta t^2 F_0 F_e - \frac{1}{2m} \Delta t^2 \mathrm{F}_0 F_d - \frac{1}{2m} \Delta t^2 \mathrm{F}_0 F_{ext} = &-\alpha (v_1 - v_0) F_e \Delta t \\ &-\beta (v_1 - v_0) F_d \Delta t \\ &-\gamma (v_1 - v_0) F_{ext} \Delta t. \end{aligned} \tag{14}$$

Since one of these terms scales with F_e and the other with F_d they can be equated separately, i.e.

$$-\frac{1}{2m} \Delta t^2 \mathrm{F}_0 F_e = -\alpha (v_1 - v_0) \mathrm{F}_\mathrm{e} \Delta t. \tag{15}$$

With the applied time integration (Eq. (4)), the left-hand side can be recast into

$$-\frac{1}{2} \Delta t (v_1 - v_0) F_e = -\alpha \Delta t (v_1 - v_0) F_e, \tag{16}$$

showing that

$$\alpha = \frac{1}{2}. \tag{17}$$

An identical argument can be made to demonstrate that

$$\beta = \frac{1}{2} \text{ and } \gamma = \frac{1}{2}. \tag{18}$$

It can now be concluded that the elastic potential energy of the system at time t_1 is given by

$$E_{el,1} = \left(v_0 + \frac{1}{2m} F_0 \Delta t\right) F_{e,0} \Delta t \,. \tag{19}$$

For an arbitrary time t_j the sum over all time steps needs to be taken, yielding, using identical arguments for the all energy types,

$$E_{el,\mathrm{j}} = \sum_{i=0}^{j-1} \left(v_\mathrm{i} + \frac{1}{2m} F_i \Delta t\right) F_{e,i} \Delta t \,,$$

$$E_{d,\mathrm{j}} = \sum_{i=0}^{j-1} \left(v_\mathrm{i} + \frac{1}{2m} F_i \Delta t\right) F_{d,i} \Delta t \,,$$

$$E_{pot,\mathrm{j}} = \sum_{i=0}^{j-1} \left(v_\mathrm{i} + \frac{1}{2m} F_i \Delta t\right) F_{ext,i} \Delta t + E_{pot,0} \,. \tag{20}$$

2.2 Verlet scheme

The most commonly used time integration scheme in LIGGGHTS® is the so-called velocity Verlet scheme, which changes the time integration to

$$v_{i+\frac{1}{2}} = v_i + \frac{\Delta t}{2\, m_i} F\left(x_i, v_{i-\frac{1}{2}}\right), \tag{21}$$

$$x_{i+1} = x_i + \Delta t\, v_{i+\frac{1}{2}}, \tag{22}$$

$$v_{i+1} = v_{i+\frac{1}{2}} + \frac{\Delta t}{2\, m_i} F\left(x_{i+1}, v_{i+\frac{1}{2}}\right). \tag{23}$$

The goal is to extract the energy information at the end of each time step. To achieve this, one time step will be viewed as two half steps for the velocity. This is possible because the energy formulation is independent of the position. As each of these half steps are Euler steps we can reuse the results of the previous section. Due to the similarity of the different energy components only E_{el} will be considered in the following. The change in elastic energy in a full Euler step is given by

$$\Delta E_{el,i-1,i} = E_{el,i} - E_{el,i-1} = \left(v_i + \frac{1}{2m} F_i \Delta t\right) F_{e,i} \Delta t \,, \tag{24}$$

as shown in Eq. (19). For the half Euler step that integrates v_i to $v_{i+1/2}$ the change in elastic energy is thus

$$\Delta E_{el,i,i+\frac{1}{2}} = \left(v_i + \frac{1}{2m} F_i \frac{\Delta t}{2}\right) F_{e,i} \frac{\Delta \mathrm{t}}{2} \,. \tag{25}$$

Similarly, integrating v from time $i + 1/2$ to $i + 1$ yields

$$\Delta E_{el,i+\frac{1}{2},i+1} = \left(v_{i+\frac{1}{2}} + \frac{1}{4m} F_{i+1} \Delta t\right) F_{e,i+1} \frac{\Delta \mathrm{t}}{2} \,. \tag{26}$$

Thus, the change of elastic energy over the full Verlet time step becomes

$$\Delta E_{el,i,i+1} = \left(v_i + \frac{1}{4m} F_i \Delta t\right) F_{e,i} \frac{\Delta t}{2} + \left(v_{i+\frac{1}{2}} + \frac{1}{4m} F_{i+1} \Delta t\right) F_{e,i+1} \frac{\Delta t}{2}. \tag{27}$$

Consequently, the energies at a time step j, for all different energy types considered, are given by

$$E_{el,\mathrm{j}} = \sum_{i=0}^{j-1} \left(v_i + \frac{1}{4m} F_i \Delta t\right) F_{e,i} \frac{\Delta t}{2} + \left(v_{i+1/2} + \frac{1}{4m} F_{i+1} \Delta t\right) F_{e,i+1} \frac{\Delta t}{2},$$

$$E_{d,\mathrm{j}} = \sum_{i=0}^{j-1} \left(v_i + \frac{1}{4m} F_i \Delta t\right) F_{d,i} \frac{\Delta t}{2} + \left(v_{i+1/2} + \frac{1}{4m} F_{i+1} \Delta t\right) F_{d,i+1} \frac{\Delta t}{2},$$

$$E_{pot,\mathrm{j}} = \sum_{i=0}^{j-1} \left(v_i + \frac{1}{4m} F_i \Delta t\right) F_{ext,i} \frac{\Delta t}{2} + \left(v_{i+1/2} + \frac{1}{4m} F_{i+1} \Delta t\right) F_{ext,i+1} \frac{\Delta t}{2} + E_{pot,0}\,. \tag{28}$$

3 DEM MODELS

In Section 4, several example simulations will be shown using the DEM models described in the following. The model responsible for the normal force is the standard Hertz-Mindlin [D04] model which is given as

$$F_e = \frac{4}{3} Y^* \sqrt{\|\delta_{ij}\| \, r_{ij}^*}\, \delta_{ij}\,, \tag{29}$$

$$F_d = -2 \sqrt{\frac{5}{6}} \beta \sqrt{S_n m^*}\, v_{ij,n} n_{ij}, \tag{30}$$

where Y^*, r_{ij}^* and m^* are the effective Young's modulus, radius and mass, δ_{ij} (> 0) and n_{ij} the distance and normal vector between the contact points, $v_{ij,n}$ the relative normal velocity and

$$\beta = \frac{\ln(e)}{\sqrt{\ln(e)^2 + \pi^2}}\,, \tag{31}$$

with e being the coefficient of restitution. Finally,

$$S_n = 2\, Y^* \sqrt{r_{ij}^* \|\delta_{ij}\|}\,. \tag{32}$$

The tangential model is the simplistic "no history" model [5], which assumes no spring in tangential direction, i.e. $F_e = 0$, giving only a contribution to the tangential dissipative force via

$$F_d = -2 \sqrt{\frac{5}{6}} \beta \sqrt{S_t m^*}\, \left(v_{ij} - v_{ij,n} n_{ij}\right), \tag{33}$$

where

$$S_t = 8\, G^* \sqrt{r_{ij}^* \|\delta_{ij}\|}\ , \tag{34}$$

and G^* is the effective shear modulus. Similarly, the lubrication model [6] also only defines a dissipative force given as

$$F_d = -\,6\,\pi\,\mu \frac{r_{ij}^2}{\|\delta_{ij}\|} v_{ij,n}\ , \tag{35}$$

where μ is the fluid viscosity and r_{ij} is the harmonic mean between the two particle radii. This force is active only if $\frac{2\,r_{ij}}{1000} < \|\delta_{ij}\| < 2\,r_{ij}$.

The bond model [7] is a combination of a normal and tangential spring-damper system that acts, even if overlaps are smaller than zero. The elastic force in normal direction is given as

$$F_e = k_n A \left(r_0 - x_{ij}\right), \tag{36}$$

where r_0 is the initial particle distance upon bond creation, x_{ij} is the distance between the particle centers, k_n the normal bond stiffness parameter and A the beam area, dependent on the beam radius which is a user defined multiple of the minimum particle radius. The elastic force in tangential direction is incrementally defined as

$$F_{e,i} = F_{e,i-1} + k_t\, A \left(v_{ij} - v_{ij,n} n_{ij}\right) \Delta t\ , \tag{37}$$

where k_t is the tangential bond stiffness parameter. Instead of using a traditional damping mechanism based on the velocity, a dissipative model is used. It reduces the elastic force in normal and tangential direction each time-step, i.e.

$$F_{e,i} = F_{e,i} \left(1 - \frac{\Delta t}{\Delta t_d}\right), \tag{38}$$

where Δt_d is the dissipation time scale and it should be noted that r_0 is adapted in normal direction, to reflect this dissipation. The dissipative force is then given as

$$F_d = F_{e,i} \frac{\Delta t}{\Delta t_d}\ . \tag{39}$$

Finally, care must be taken when contacts end, e.g. bonds are broken, as in that case the elastic potential is instantaneously converted into dissipated energy.

4 DEMONSTRATION

In the following a few basic test cases are shown, demonstrating the exactness of the developed formulae.

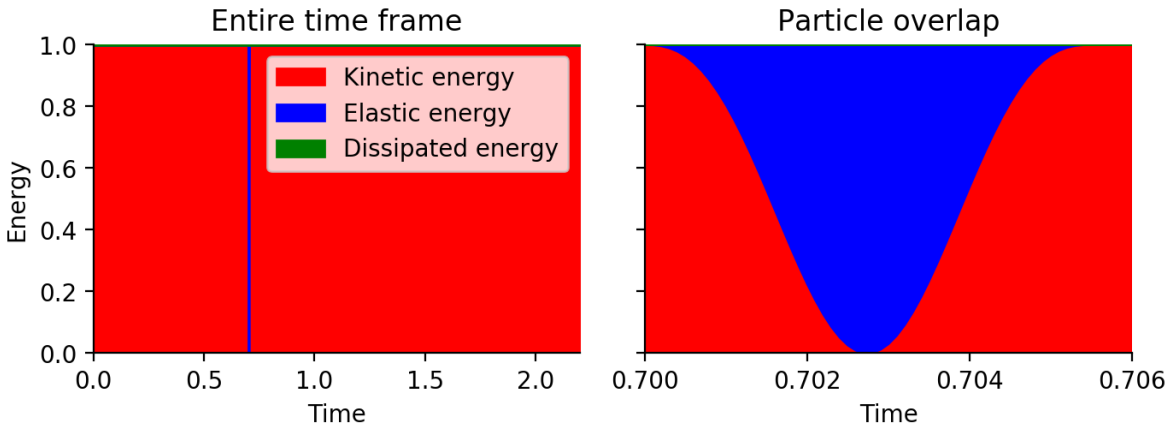

***Figure 1**: Energy balance for the normal contact of two particles*

4.1 Normal contact

In this case two particles of identical radius r and mass m are placed $2.2\,r$ apart. Their initial velocity is identical, except for the orientation. The coefficient of restitution is 1.0, i.e. no damping takes place and only the Hertz-Mindlin normal model will be active. In the following, all velocities and time scales are normalized with the initial particle velocity and radius. Figure 1 shows the kinetic, elastic and dissipated energy components over time. While the left pictures shows the whole time frame, the right shows the short period where the two particles overlap, i.e. when the normal model is active. It can be seen that the entire kinetic energy is converted to elastic energy until the point of maximum overlap. Afterwards, the the spring relaxes and the particles return to their original kinetic energy. Due to no damping, the dissipated is expected to remain zero. However, the elastic potential at the end of the contact is approximately 10^{-7}, showing that this model does not conserve energy perfectly. As this remaining elastic energy is dependent on the time step size it is clear that a numerical error is at the core of this mismatch. Similar behaviour was observed by [8]. Note that this does not

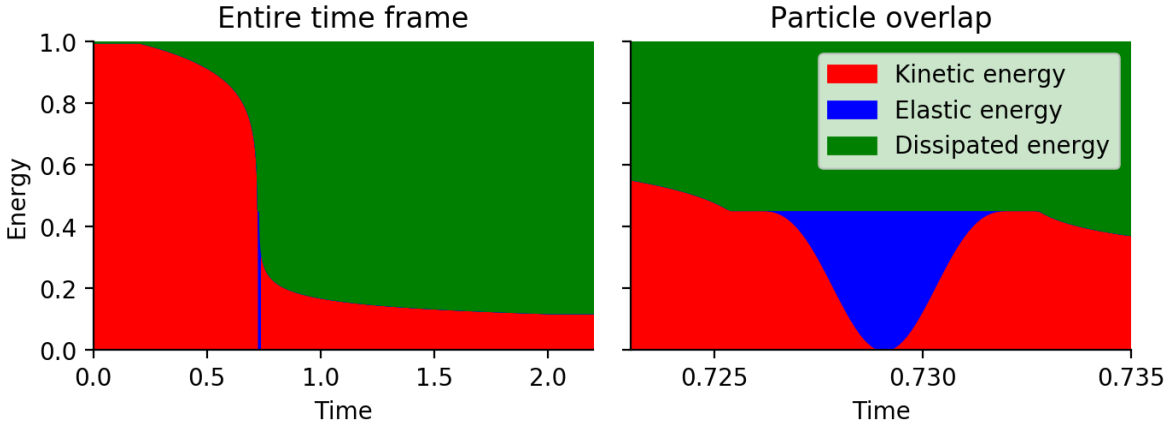

Figure 2: Energy balance of a particle contact using a lubrication model

change the present energy computation as this remaining elastic energy gets assigned to the dissipated energy value. Thus, it should be appreciated that the dissipated energy contains energy from both physical as well as numerical dissipation.

4.2 Normal contact with lubrication

The setup is identical to the previous case, except for the additional activation of the lubrication model. Compared to Figure 1, Figure 2 now shows the clear influence of the dissipation model, which significantly removes kinetic energy from the system. There is also a brief overlap of the particles, which is shown in detail in the right-hand-side figure. The brief constant areas of dissipation before the actual contact show the cut-off value of the lubrication model.

4.3 Bonded particles

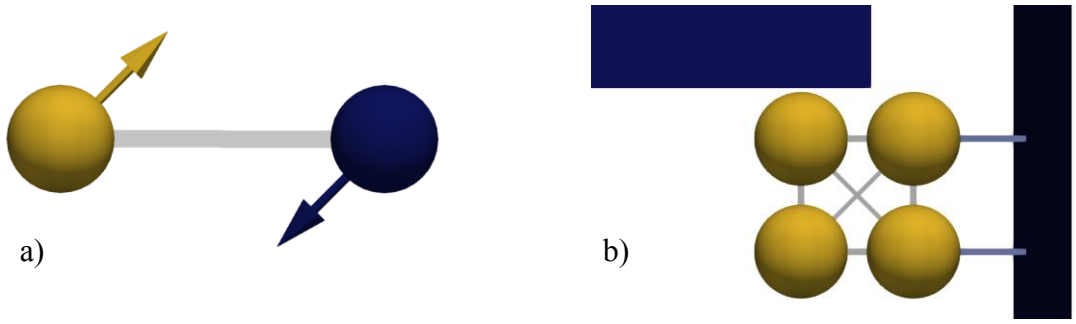

Figure 3: a) Setup of bonded particle case; b) Setup of case with bonded particles impacted by a wall

The setup for this case is similar to the one in Section 4.1. This time the bond model, including dissipative terms, is activated and the particles have a relative tangential velocity, which causes them to rotate. Figure 3a shows the initial state of the simulation with established bond. While rotations have not been treated in the derivation above, the extension is straightforward to include the angular kinetic energy and torques. The initial tangential

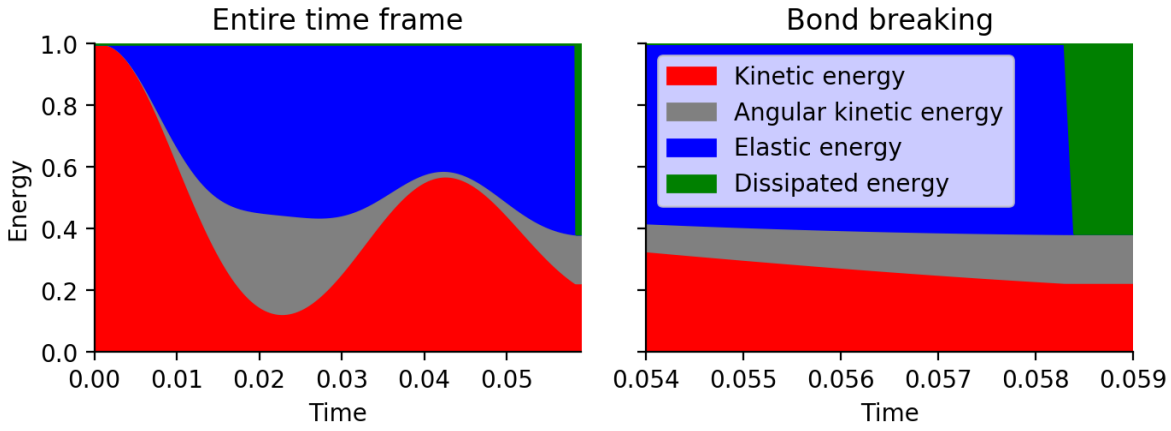

Figure 4: Energy balance of two bonded particles

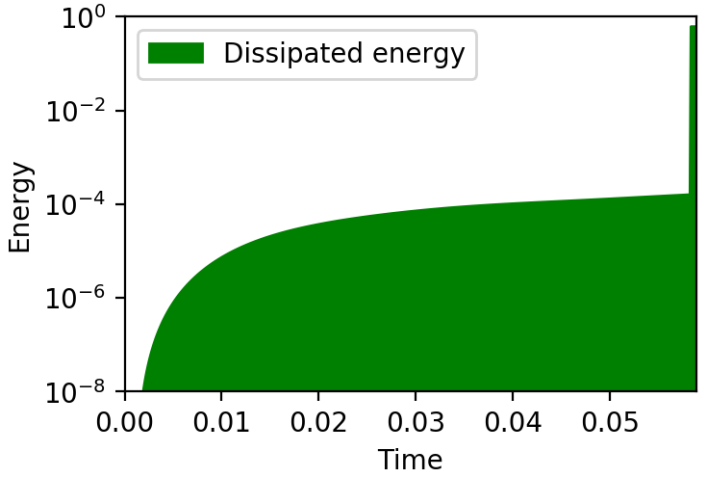

Figure 5: Dissipated energy during the interaction of two bonded particles

movement of the two particles causes the bond beam to rotate and induce an angular kinetic energy into the system as shown in Figure 4. The bond is designed such that the particles break when their distance is 1% larger than the initial distance. This is shown in detail on the right-hand-side of Figure 4, where the instantaneous conversion from elastic to dissipated energy takes place, followed by constant kinetic energies. Even though the dissipation model is active the effect during the time when the particles are bonded is rather low. Figure 5 shows the dissipated energy in a lin-log plot to demonstrate the effect of the model.

4.4 Bonded wall impact

The setup for this case can be seen in Figure 3b. Two particles are bonded with the right wall and the four particles are interconnected with bonds that can break if a stress magnitude is exceeded. The wall on the top left is a solid object with an initial velocity that has the freedom to accelerate in movement direction. Figure 6 shows the only 2 % of the total energy, as the kinetic energy of the wall fills the remainder. The light blue and green parts show the

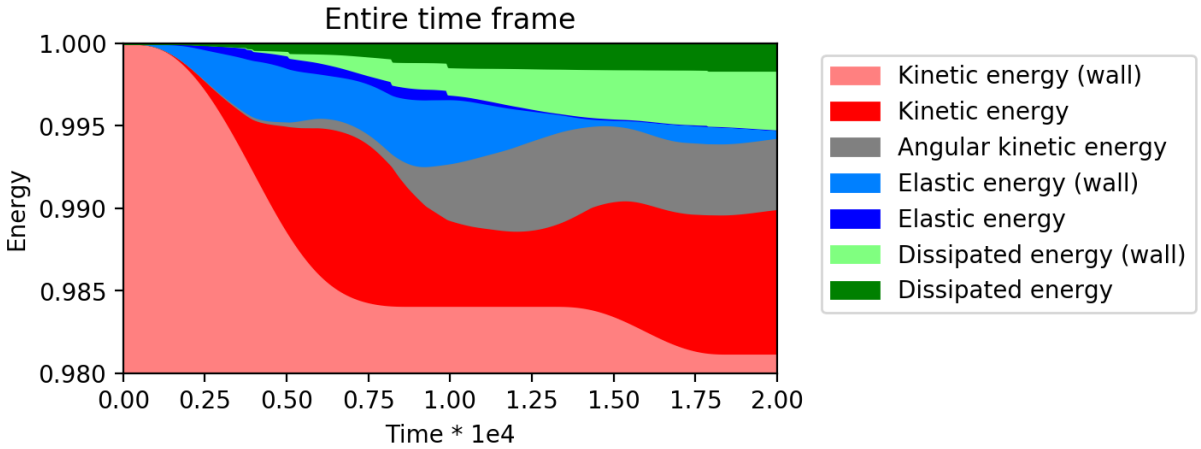

Figure 6: Energy balance during the impact of a wall onto bonded particles

elastic and dissipated energy between particle-wall contacts, whereas the dark ones show the associated energies for the particle-particle contacts. The jumps in elastic energy clearly show the breaking of the particle-particle bonds and the dissipated energy between wall and particles show the large damping occurring between the two. It should be noted that for all the calculations performed in Section 4 the total energy is preserved up to numerical epsilon.

5 CONCLUSION

The discrete element method mostly uses spring damper systems to represent different physical particle-particle and particle-wall interactions. In this paper, the equations for the energy balance of such systems was described for standard Euler integration and velocity Verlet schemes. It was shown that the use of the correct velocity needs to be used in order to guarantee energy conservation. The developed formulae were then applied to standard DEM models, showing their practical applicability. Finally, four different test cases were shown to demonstrate the validity of the developments. The last case exhibited 7 different energy types when a wall collided with four bonded particles.

The analysis of such a complex interplay in real-world applications will allow to gain further insight into the mechanics of particle systems. Examples are all types of particle-solid interactions, such as a stone impacting the seabed or the energy required to dredge the seabed. Additionally, the energies can be used as input into other models, e.g. the dissipated energy as source term for heat-conduction models. The test case with only a normal model has also shown that the present formulation allows to identify potential numerical energy losses in DEM models. This can allow model reformulations or development of correction terms.

REFERENCES

[1] P. A. Cundall and O. D. L. Strack, “A discrete numerical model for granular assemblies,” Géotechnique, vol. 29, no. 1, pp. 47–65, Mar. 1979.

[2] S. Luding, E. Clément, A. Blumen, J. Rajchenbach, and J. Duran, “Anomalous energy dissipation in molecular-dynamics simulations of grains: The ``detachment'' effect,” Phys. Rev. E, vol. 50, no. 5, pp. 4113–4122, Nov. 1994.

[3] B. N. Asmar, P. A. Langston, A. J. Matchett, and J. K. Walters, “Energy monitoring in distinct element models of particle systems,” Advanced Powder Technology, vol. 14, no. 1, pp. 43–69, Feb. 2003.

[4] S. Siiriä and J. Yliruusi, “Particle packing simulations based on Newtonian mechanics,” Powder Technology, vol. 174, no. 3, pp. 82–92, May 2007.A. Di Renzo and F. P. Di Maio, “Comparison of contact-force models for the simulation of collisions in DEM-based granular flow codes,” Chemical Engineering Science, vol. 59, no. 3, pp. 525–541, Feb. 2004.

[5] A. Di Renzo and F. P. Di Maio, “Comparison of contact-force models for the simulation of collisions in DEM-based granular flow codes,” Chemical Engineering Science, vol. 59, no. 3, pp. 525–541, Feb. 2004.

[6] W. Zhang, R. Noda, and M. Horio, “Evaluation of lubrication force on colliding particles for DEM simulation of fluidized beds,” Powder Technology, vol. 158, no. 1–3, pp. 92–101, Oct. 2005.

[7] D. O. Potyondy and P. A. Cundall, “A bonded-particle model for rock,” International

Journal of Rock Mechanics and Mining Sciences, vol. 41, no. 8, pp. 1329–1364, Dec. 2004.

[8] D. Zhang and W. J. Whiten, “An efficient calculation method for particle motion in discrete element simulations,” Powder Technology, vol. 98, no. 3, pp. 223–230, Aug. 1998.